CHAPTER V
FABRICATION OF TITANIUMDIOXIDE/PURIFIED SODIUM-BENTONITE AND TITANIUM/CTAB-MODIFIED SODIUM-BENTONITE COMPOSITES FOR DSSC ELECTRODES

5.1 Abstract

In this work, TiO_2/purified Na-bentonite and TiO_2/CTAB-modified Na-bentonite composites were fabricated with different Si contents and calcination temperature, and applied as electrodes for dye-sensitized solar cells. The photovoltaic properties of the solar cells sensitized by red cabbage dye were determined. The results showed that the CTAB-modified Na-bentonite was more suitable to form a composite with the P25 TiO_2 in order to make a more homogeneous film, leading to a higher efficiency of the dye-sensitized solar cell. Furthermore, the use of the P25 TiO_2/Na-bentonite composite with 5 mol% Si in the form of both purified Na-bentonite and CTAB-modified Na-bentonite as electrodes provided good solar cell performances close to that of the pure P25 TiO_2 electrode. In addition, the calcination temperature of 600 °C did not change in solar cell performances compared to that of 500 °C, except for that of the cell fabricated with the P25 TiO_2/10 mol% Si purified Na-bentonite.

Keywords: Titanium dioxide, Clay, Semiconductor, Red cabbage dye, Photovoltaic properties

5.2 Introduction

Montmorillonite constituting bentonite mineral is not only used in various well-known industrial applications, such as foundry and ceramic industries, but also in catalyst industries and plastic packaging, as well as in energy fields, e.g. petroleum, nuclear, and dye-sensitized solar cell (Damardji *et al.*, 2009; Lai *et al.*, 2009; Liu *et al.*, 2006; Saelim *et al.*, 2011a; Saelim *et al.*, 2011b). It can be applied in

its natural form and after some modifications by acid, alkali, and organics (Steudel *et al.*, 2009). These all usages are mainly because of its electrical surface charges, which govern chemical characteristic and physical phenomena, such as ion exchange, adsorption, swelling, colloidal stability, and flow behaviors (Duc *et al.*, 2005). The electrical charge of montmorillonite can be generated by two ways: (1) charge-imbalanced substitutions in the crystalline network of $Mg^{2+}$for Al^{3+}in octahedral coordination, resulting in positive charge defects and then obtaining negative charges, and (2) bond dissociation of the outermost oxygen and hydroxyls bound to the metal cations (e.g. Si, Al, and Mg) at the edge surfaces (Velde, 1995). With its surface properties and platelet structure, this is also promising for solar cells application like dye-sensitized solar cell consisting of several components in which could be incorporated with clay.

Since the Grätzel's cell or dye-sensitized solar cell (DSSC) (Barbé *et al.*, 1997; Kalyanasundaram *et al.*, 1998; Nazeerudin *et al.*, 1993) has many advantages in indoor application over the conventional silicon solar cell, especially its capability of converting low light intensity to electricity, it is a very potential solar cell in the near future. According to our previous work (Saelim *et al*, 2011a), the modified natural Na-bentonite, studied possessing an aluminosilicate structure with platelet size less than 2 μm was found interestingly to exhibit as an energy barrier (Nguyen *et al.*, 2007) characteristic for suppression of charge recombination due to their insulation property (Kumara *et al*, 2001; Palomares *et al.*, 2003) and induce a multiple light scattering (Park *et al.*, 2008). However, clay insulating phenomenon of the cell fabricated with the P25 TiO_2/15 mol%Si CTAB-modified Na-bentonite composite was quite more evident than the energy barrier and light scattering phenomena (Saelim et al, 2011a). This is mainly because of a too much bentonite content used to form the composite. In addition, bentonite or clay is a flame retardant so it is hard to burn organic substance on clay surface at the normal temperature. As a result, calcinations temperature at 500 °C provided some char residual from surfactant (CTAB) used to modify bentonite surface. This char could absorb some visible light and its absorption might compete with light absorption of dye molecules. Therefore, the optimization of bentonite content (i.e. Si content) and char removal should be further investigated to obtain a higher solar cell performance.

In the present work, two Na-bentonite forms with different surface polarities (i.e. purified Na-bentonite and CTAB-modified Na-bentonite) were used to fabricate the P25 TiO_2/Na-bentonite composites as photoelectrode for dye-sensitized solar cells. Two different bentonite contents (in terms of Si contents) of 5 and 10 mol% (i.e. Ti:Si molar ratio of 95:5 and 90:10, respectively) were employed. Natural red cabbage dye was utilized as the sensitizer of the DSSCs. To remove char residual, influence of use of higher calcination temperature and non-modified bentonite (purified Na-bentonite) for the TiO_2/bentonite composite preparation on the solar cell performances was examined.

5.3 Experimental

5.3.1 Materials

Na-bentonite 70% purity was kindly supplied from Thai Nippon Chemical Industry Co., Ltd, Thailand. Cetyltrimethylammoniumbromide (CTAB) 99+%, acetylacetone 99.3% and triton® X-100 were from ACROS. Commercial P25 TiO_2 powder was from Degussa. Polyethylene glycol (MW of 20,000) was from Fluka. LiI 99%, 4-tert-butylpiridine 96% and chloroplatinic acid hydrate ~38% Pt-basis were from Sigma-Aldrih, and I_2 was from Suksapanpanish, Thailand.

5.3.2 Preparation of Red Cabbage Dye Sensitizer

Fresh red cabbage leaves were cut into very small pieces and then extracted in a methanol/water (3:1 by volume) mixed solvent. Afterward, the solid residues were filtered out. Then, the dye solution was concentrated by a rotary evaporator at 50 °C and finally stored at 4 °C prior to use.

5.3.3 Preparation of Purified Na-Bentonite

Raw Na-bentonite was purified more by swelling in deionized water with 30 times by weight under vigorous stirring for 12 h. The swollen Na-bentonite was centrifuged at 10,000 rpm for 10 min. Then, the supernatant containing highly dispersed swollen Na-bentonite, which had the main compositions of 78.5 wt.% SiO_2, 16.4 wt.% Al_2O_3, 2.4 wt.% Fe_2O_3, and 1.7 wt.% MgO obtained from the X-ray

fluorescence analysis, was collected, dried, and ground in mortar. The purified Na-bentonite was attained.

5.3.4 Preparation of CTAB-Modified Na-Bentonite

The method to prepare the CTAB-modified Na-bentonite was described in our previous work (Muksing *et al.*, 2008). The mixture of the CTAB surfactant in aqueous solution with 1.5 equivalents of CEC and the swollen purified Na-bentonite was mixed vigorously at 80 °C for 2 h and homogenized at 80 °C for 30 minutes. Afterwards, the modified Na-betonite was filtered, washed several times with hot water and dried in an oven. Then, the modified clay was ground and screened through 325 mesh sieve.

5.3.5 Preparation of Photoanodes

The pure TiO_2 paste, 1 g of the TiO_2 powder with 0.1 ml of acetylacetone, 0.4 ml of Triton X-100, and 0.5 g of polyethylene glycol (MW of 20,000) in 5 ml of a mixture of water and ethanol was prepared under sonication. In the case of P25 TiO_2/Na-bentonite composites, with 5 and 10 mol%Si contents, all additives were used as the same ratio as in case of the pure TiO_2 paste, thereby mixed powder of P25 and bentonite was counted as equal to pure P25. To obtain the homogenized pastes easier, in case of TiO_2/purified Na-bentonite, the purified Na-bentonite was dispersed first in water but in case of TiO_2/CTAB-modified Na-bentonite, the CTAB-modified Na-bentonite was dispersed first in ethanol before mixed with P25 and then other chemicals. Afterwards, the paste was spread on fluorine-doped SnO_2 (FTO) glasses (Pilkington TEC15, sheet resistance of 15 Ω/cm^2) by the doctor blading method with 1.0 cm^2 area and calcined at 500 and 600 °C for 1 h. Then, the calcined film was immersed into the extracted red cabbage dye solution for 20 h to obtain the photoanode film.

5.3.6 Cell Assembly

To assemble the cell, the 80 μm-thick transparent sticker film was used as spacer to make a narrow empty space inside the cell between the as-prepared semiconductor photoanode film and the Pt cathode film. The Pt cathode film was

prepared by spreading 1 drop of 7 mM chloroplatinic acid hydrate in 2-propanol by the doctor blading method on fluorine-doped SnO_2 (FTO) glasses (sheet resistance of 15 Ω/cm^2) and annealed at 400 °C for 30 min. The electrolyte consisting of 0.3 M LiI, 0.015 M I_2, and 0.1 M 4-tert-butylpiridine in acetonitrile was dropped and spread thoroughly in the as-prepared space between the two electrodes. Two clips were used to camp two electrodes together. The photovoltaic measurement was performed suddenly after electrolyte spreading.

5.3.7 Characterization and Measurement

The physical properties of photoanodes were characterized by using a field emission scanning electron microscope (FE-SEM, Hitachi S4800), a polarized optical microscope (DMRXP, LEICA) and a N_2 adsorption-desorption analyzer (Autosorb-1, Quantachrome). The photovoltaic properties of the prepared DSSCs, i.e. short circuit current (J_{sc}, mA/cm^2), open circuit voltage (V_{oc}, V), fill factor (FF), and efficiency (η, %), were determined from the I–V curve obtained by using a digital Keithley 236 multimeter under an irradiation of white light from a 1000 W/HS Xenon arc lamp with a 100 mW/cm^2 light intensity, where the fill factor and efficiency were calculated based on the following equations:

$$FF = \frac{J_{max} \times V_{max}}{J_{sc} \times V_{oc}} \tag{5.1}$$

$$\eta = \frac{J_{sc} \times V_{oc} \times FF}{P_{in}} \tag{5.2}$$

where J_{max} is maximum power point current (mA/cm^2), V_{max} is maximum power point voltage (V), and P_{in} is power of incident light (mW/cm^2).

5.4 Results and Discussion

FE-SEM micrographs in Fig. 5.1 show different morphology of the electrodes fabricated with the P25 and the P25 TiO_2/bentonite composites. It was observed that macropores of 1-2 μm were formed in the pure P25 electrode (Fig. 5.1a) due to the decomposition of a large amount of 50 wt.% polyethylene glycol used during the paste preparation step (Barbé et al., 1997). However, these large pores could not be found in composite electrodes (Fig. 5.1b and c). This might possibly due to the adsorption of some polyethylene glycol on both kinds of bentonite surfaces, subsequently reduction in polymer droplet size in the media and in the composite after calcinations process. Nevertheless, the morphology of the P25 TiO_2/purified Na-bentonite and P25 TiO_2/CTAB-modified Na-bentonite composites at both bentonite contents does not show any difference. The cross-sectional FE-SEM image of composite at high magnification is shown in Fig. 5.1d. Besides, a high dispersion of both bentonite clays in the composite films at both bentonite contents was clearly observed.

On the other hand, the observation of the films by using an optical microscope shows that the films fabricated with the P25 TiO_2 (Fig. 5.2a) and P25 TiO_2/CTAB-Na-modified bentonite (Fig. 5.2c.) are more homogeneous than that fabricated with the P25 TiO_2/purified Na-bentonite (Fig. 5.2b.). This implies that some dense aggregates were formed in a larger scale, namely the bright part on the optical microscopy image of the film fabricated with the P25 TiO_2/purified Na-bentonite indicates the less transparent parts of the film. This phenomenon could be observed from its paste mixture, in which the particles flocculated, rapidly settled down and left clear solution on the top. It was attributed to negatively charges on the purified Na-bentonite surface (Duc *et al.*, 2005), accordingly raising pH of the media close to the isoelectric point of P25 TiO_2 particle (pH of 5.5) (Barbé et al., 1997).

The specific surface areas, as shown in Table 5.1, of both the P25 TiO_2/purified Na-bentonite and the P25 TiO_2/CTAB-modified Na-bentonite composites were significantly higher than that of the pure P25 TiO_2, which agree well with our previous work (Saelim et al., 2011a; Saelim et al., 2011b). At 500 °C,

the specific surface area of composite with purified Na-bentonite increases with bentonite content, and this is in accordance with our previous work (Saelim et al., 2011b), which the composites of sol-gel TiO_2/purified Na-bentonite were investigated. On the contrary, 10 mole% Si CTAB-modified Na-bentonite exhibits lower specific surface area than composite with 5 mole% Si CTAB-modified Na-bentonite, but this trend is reversed at the calcination temperature of 600 °C. This is attributed to the effect of CTAB-derived residual carbon on clay surface at the high CTAB-modified Na-bentonite content (Acronada *et al.*, 2009) since less of CTAB-derived residual carbon was left at higher calcinations temperature and let bentonite clay platelets inhibit TiO_2 particle agglomeration from sintering effect (Saelim et al., 2011a; Saelim et al., 2011b). Meanwhile, the specific surface areas of the 10 mol% Si purified Na-bentonite composite was quite lower than that of 10 mol% Si CTAB-modified Na-bentonite composite at the calcination temperature of 600 °C because increase in purified Na-bentonite content resulted in more particles agglomeration, therefore high TiO_2 sintering and then less exposed area.

Table 5.2 reveals the photovoltaic properties of DSSCs sensitized by red cabbage dye with photoanode thickness of about 6 μm. After calcination temperature of 500°C, the overall photovoltaic properties tend to decrease when the bentonite content increases. This reveals that besides the insulation property of clay platelets, they also retarded the ion diffusion in electrolyte as the same effect of high electrolyte viscosity, and this consequently led to a lower current and fill factor, such explained by Hagfeldt *et al* (1994).

Although the purified Na-bentonite provided lower photovoltaic properties than the CTAB-modified Na-bentonite, the photovoltaic properties of 5 mol% Si purified Na-bentonite and 5 mol% Si CTAB-modified Na-bentonite electrodes were insignificantly different. The very low photovoltaic properties of the 10 mol% Si purified Na-bentonite electrode compared to 10 mol% Si CTAB-modified Na-bentonite might be due to the inhomogeneous characteristic of the film. The large number of aggregates could result in too much back-scattering (Ferber and Luther 1998) and also hinder the light absorption of dye molecules.

Considering calcinations temperature at 600 °C compared with at 500 °C, a similar trend of different kind of composite electrodes is found, and a bit lower fill factor in most cells is observed due to higher resistivity of conductive layer on conducting glass (Ngamsinlapasathian *et al.*, 2006). The cell performances of composite with 5 mole% Si of both bentonites are not significantly different with different calcinations temperature. The quite lower cell performance of 10 mol% Si purified Na-bentonite electrode is owing to its high sintering at higher calcinations temperature and less homogeneous characteristics as described above at 500 °C calcinations temperature. In contrast, the higher cell performance due to higher photocurrent of 10 mol% Si CTAB-modified Na-bentonite is attributed to less char residual in the electrode. This less char residual is needed to allow dye molecules to absorb more visible light since its back color could absorb some light in visible region (Tang *et al.*, 2010; Yen *et al.*, 2008).

On the other hand, the char residual is considered as a mixture of carbon allotropes containing amorphous carbon and microscopic crystals of graphite-like (Vander Wal, 1996). Its conductivity is probably in the order of 10^{-7} S/m as reported in coal char pyrolyzed under argon atmosphere at 500°C (Duba, 1977) or higher regarding its carbon content. Meanwhile, the graphene sheet, a layer of graphite (Tang *et al.*, 2010; Yang *et al.*, 2010) employed in dye-sensitized solar cells was considered as electron acceptors since it was able to receive photo-injected electrons from the conduction band of TiO_2, and especially conducted electrons along their structure as a new electron pathway to the back electrode. This improves photocurrent of the cells due to its excellent electron conducting (Conductivity of graphene ~10^{-3}-10^{2} S/m) (Kong *et al.*, 2009; Worsley *et al.*, 2010). Thus, it was possible that electrons transferred from the conduction band of TiO_2 to this char residual, and electron transportation in this conductive carbon might occur as well. However, the photocurrents of composite electrodes in this study do not improve. Therefore, it can be concluded that, low light adsorption of dye molecules owing to visible light absorption of the char residual is more dominant than electron conducting in the char residual which has quite low electrical conductivity compared to that of graphene.

In summary, 5 mol% Si bentonite content in TiO_2 electrode did not diminish much the performance of DSSCs, as it has low clay content, low char residual and homogeneous film. Moreover, CTAB-modified Na-bentonite did not cause inhomogeneous characteristic in the electrode due to suppression of the electronic charges on its surface by surfactant. Meanwhile, the pH controlling in P25 TiO_2/purified Na-bentonite paste is needed for high dispersion of TiO_2 particles and homogeneous composite electrodes. Although purified Na-bentonite and calcinations temperature at 600 °C succeeded to remove some char residual in the electrodes, pH controlling in the paste media is essential to render a homogeneous electrode film with purified Na-bentonite as well as higher calcinations could deteriorate FTO glasses conductivity and influence TiO_2 phase formation and TiO_2 particle size. The other efficient techniques are needed in the future work. Besides, various preparation methods to improve the electronic contact of TiO_2 and between TiO_2 and both kinds of bentonite are the challenging parts in the further studies.

5.5 Conclusions

In this work, 5 and 10 mol% Si of the P25 TiO_2/purified Na-bentonite and the P25 TiO_2/CTAB-modified Na-bentonite composites were investigated as photoelectrodes for DSSCs compared to P25 TiO_2 electrode. The red cabbage dye was employed as the sensitizer of the DSSCs. Besides, the performances of DSSCs with two different calcination temperatures of 500 °C and 600 °C were also determined. Even though the photovoltaic properties of composite electrodes were attenuated with higher bentonite content, they were not suppressed much with 5 mol% Si bentonite content in composite electrodes. Furthermore, CTAB-modified Na-bentonite was more suitable to form a composite with the P25 TiO_2 electrode without pH controlling in the paste media. In addition, the char residual was able to be removed by using purified Na-bentonite or high calcinations temperature but both of them still have some drawbacks. Thus, other methods are required in the further studies.

5.6 Acknowledgments

This work was financially supported by the Royal Golden Jubilee Ph.D. Program, Thailand; Rachadapiseksompote Endowment, Chulalongkorn University, Thailand; and National Nanotechnology Center, National Science and Technology Development Agency, Thailand. The authors also would like to thank Thai Nippon Chemical Industry Co., Ltd for kindly providing the clay and thank Asst. Prof. Thammanoon Sreethawong for proof reading the article.

5.7 References

Acronada, N., Durán, A., Suárez, S., Portela, R., Coronado, J.M., Sánchez, B., and Castro, Y. (2009). Synthesis and photocatalytic properties of dense and porous TiO_2-anatase thin films prepared by sol–gel. Applied Catalysis B: Environmental, 86(1-2), 1-7.

Barbé, C.J., Arendse, F., Comte, P., Jirousek, M., Lenzmann, F., Shklover, V., and Grätzel, M. (1997). Nanocrystalline titanium oxide electrode for photovoltaic applications. Journal of the American Ceramic Society, 80(12), 3157-3171.

Damardji, B., Khalaf, H., Duclaux, L., and David, B. (2009). Preparation of titaniapillared montmorillonite as photocatalyst Part I. Microwave calcination, characterization, and adsorption of a textile azo dye. Applied Clay Science, 44(3-4), 201-205.

Duba, A. G. (1977). Electrical conductivity of coal and coal char. Fuel, 56(), 441-443.

Duc, M., Gaboriaud, F., and Thomas, F. (2005). Sensitivity of the acid-base properties of clays to the methods of preparation and measurement 1. Literature review. Journal of Colloid and Interface Science, 289(1), 139-147.

Ferber, J., and Luther, J. (1998). Computer simulations of light scattering and absorption in dye-sensitized solar cells. Solar Energy Materials & Solar Cells, 54(1-4), 265-275.

Hagfeldt, A., Didriksson, B., Palmqyist, T., Lindström, H., Södergren, S., Rensmo, H., and Lindquist, S.-E. (1994). Verification of high efficiencies for the Grätzel–cell. A 7% efficient solar cell based on dye-sensitized colliodal TiO_2 film. Solar Energy Materials & Solar Cells, 31(4), 481-488.

Kalyanasundaram, K., and Grätzel, M. (1998). Application of functionalized transition metal complexes in photonic and optoelectronic devices. Coordination Chemistry Reviews, 177(1), 347-414.

Kong, B.-S., Yoo, H.-W., and Jung, H.-T. (2009). Electrical conductivity of graphene films with a poly(allylamine hydrochloride) supporting layer. Langmuir, 25 (18), 11008-11013.

Kumara, G.R.R.A., Tennakone, K., Perera, V.P.S., Konno, A., Kaneko, S., and Okuya, M. (2001). Suppression of recombinations in a dye-sensitized photoelectrochemical cell made from a film of tin IV oxide crystallites coated with a thin layer of aluminium oxide. Journal of Physics D: Applied Physics, 34(6), 868-873.

Lai, Y.-H., Chiu, C.-W., Chen, J.-G., Wang, C.-C., Lin, J.-J., Lin, K.-F., and Ho, K.-C. (2009). Enhancing the performance of dye-sensitized solar cells by incorporating nanosilicate platelets in gel electrolyte. Solar Energy Materials & Solar Cells, 93(10), 1860-1864.

Liu, S., Yang, J.-H., and Choy, J.-H. (2006). Microporous SiO2-TiO2 nanosols pillared montmorillonite for photocatalytic decomposition of methyl orange. Journal of Photochemistry and Photobiology A: Chemistry, 179(1-2), 75-80.

Muksing, N., Nithitanakul, M., Grady, B.P., and Magaraphan, R. (2008). Melt rheology and extrudate swell of organobentonite-filled polypropylene nanocomposites, Polymer Testing, 27(4), 470-479.

Nazeeruddin, M.K., Kay, A., Rodicio, I., Humphry-Baker, R., Müller, E., Liska, P., Vlachopoulos, N., and Grätzel, M. (1993). Conversion of light to electricity by cis-X2bis(2,2'-bipyridyl-4,4'-dicarboxylate)ruthenium(II) charge-transfer sensitizers (X = Cl-, Br-, I-, CN-, and SCN-) on nanocrystalline TiO_2 electrodes. Journal of the American Chemical Society, 115(14), 6382-6390.

Ngamsinlapasathian, S., Sreethawong, T., and Yoshikawa, S. (2008). Enhanced efficiency of dye-sensitized solar cell using double-layered conducting glass. Thin Solid Films, 516(21), 7802-7806.

Nguyen, T.-V., Lee, H.-C., Alam Khan, M., and Yang, O.-B. (2007). Electrodrposition TiO_2/SiO_2 nanocomposite for dye-sensitized solar cell. Solar Energy, 81(4), 529-534.

Palomares, E.; Clifford, J.N.; Haque, S.A.; Lutz, T.; Durrant, J.R. (2003).Control of Charge Recombination Dynamics in Dye Sensitized Solar Cells by the Use of Conformally Deposited Metal Oxide Blocking Layers. Journal of the American Chemical Society, 125(2), 475-482.

Park, J. H., Kim, B.-W., and Moon, J. H. (2008). Dual functions of clay nanoparticles with high aspect ratio in dye-sensitized solar cells. Electrochemical and Solid-State Letters, 11(10), B171-B173.

Saelim, N.-o., Magaraphan, R., and Sreethawong, T. (2011a). TiO_2/modified natural clay semiconductor as a potential electrode for natural dye-sensitized solar cell. Ceramics International, 37(2), 659-663.

Saelim, N.-o., Magaraphan, R., and Sreethawong, T. (2011b). Preparation of sol–gel TiO_2/purified Na-bentonite composites and their photovoltaic application for natural dye-sensitized solar cells. Energy Conversion and Management, 52(8-9), 2815-2818.

Steudel, A., Batenburg, L.F., Fischer, H.R.,Weidler, P.G., and Emmerich, K. (2009). Alteration of swelling clay minerals by acid activation. Applied Clay Science, 44(1-2), 105-115.

Tang, Y.-B., Lee, C.-S., Xu, J., Liu, Z.-T., Chen, Z.-H., He, Z., Cao, Y.-L., Yuan, G., Song, H., Chen, L., Luo, L., Cheng, H.-M., Zhang, W.-J., Bello, I., and Lee, S.-T. (2010). Incorporation of graphenes in nanostructured TiO_2 films via molecular grafting for dye-sensitized solar cell application. ACS Nano, 4(6), 3482-3488.

Vander Wal, R. L. (1996, May). Soot precursor material: Spatial location via simultaneous LIF-LII imaging and characterization via TEM. Paper presented at 1996 Technical Meeting of the Central States Section of the Combustion Institute, St. Louis, Missouri, United States of America.

Velde, B. (1995). Origin and Mineralogy of Clays: Clays and the Environment. New York: Springer-Verlag.

Worsley, M. A., Pauzauskie, P. J., Olson, T. Y., Biener, J., Satcher, J. H., Jr., and Baumann, T. F. (2010). Synthesis of graphene aerogel with high electrical conductivity. Journal of the American Chemical Society, 132(40), 14067-14069.

Yang, N., Zhai, J., Wang, D., Chen, Y., and Jiang, L. (2010). Two-dimensional graphene bridges enhanced photoinduced charge transport in dye-sensitized solar cells. ACS Nano, 4(2), 887-894.

Table 5.1 Specific surface area results of the semiconductors fabricated with P25 TiO_2 pastes containing different bentonite contents

Semiconductor	Specific surface area at calcination temperature of 500 °C (m^2/g)	Specific surface area at calcination temperature of 600 °C (m^2/g)
P25 TiO_2	61.0	54.4
P25 TiO_2/5 mol% Si purified Na-bentonite	65.3	61.9
P25 TiO_2/10 mol% Si purified Na-bentonite	67.2	61.1
P25 TiO_2/5 mol% Si CTAB-modified Na-bentonite	64.1	58.1
P25 TiO_2/10 mol% Si CTAB-modified Na-bentonite	62.3	64.7

Table 5.2 Photovoltaic properties of DSSCs sensitized by red cabbage dye with photoanode thickness of about 6 μm at 500°C

Semiconductor Electrode	Calcination temperature (°C)	J_{SC} (mA/cm^2)	V_{oc} (V)	FF	η (%)
P25 TiO_2	500*	2.25	0.60	0.35	0.46
	600*	2.22	0.60	0.34	0.44
	500	2.07	0.60	0.33	0.40
P25 TiO_2/5 mol% Si purified Na-bentonite	500	1.35	0.60	0.29	0.24
	600	1.34	0.60	0.26	0.21
P25 TiO_2/10 mol% Si purified Na-bentonite	500	0.89	0.61	0.28	0.16
	600	0.72	0.61	0.24	0.11
P25 TiO_2/5 mol% Si CTAB-modified Na-bentonite	500	1.49	0.60	0.30	0.28
	600	1.49	0.64	0.28	0.27
P25 TiO_2/10 mol% Si CTAB-modified Na-bentonite	500	1.32	0.60	0.24	0.19
	600	1.58	0.63	0.22	0.22

*Thickness of electrode was greater than 6 μm

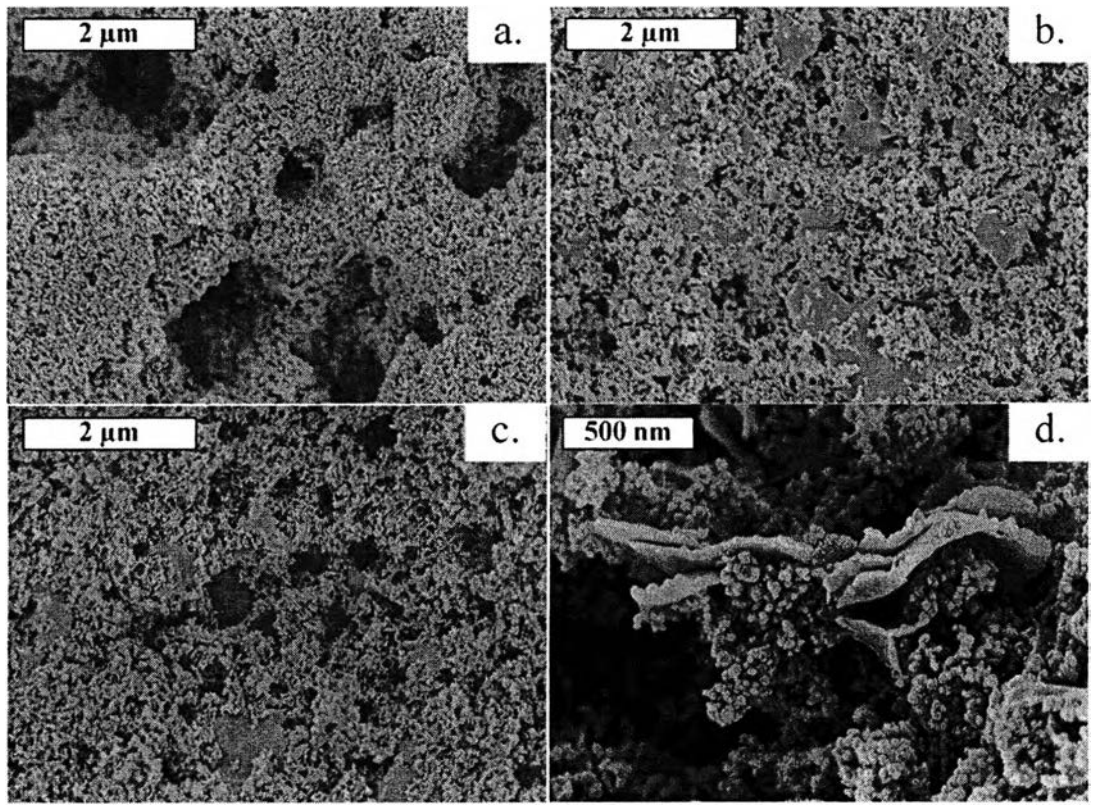

Figure 5.1 Top-viewed FE-SEM micrographs of (a) P25 TiO_2 electrode, (b) P25 TiO_2/5 mol% Si purified Na-bentonite electrode, (c) P25 TiO_2/5 mol% Si CTAB-modified Na-bentonite electrode, and cross-sectional FE-SEM micrographs of (d) P25 TiO_2/bentonite.

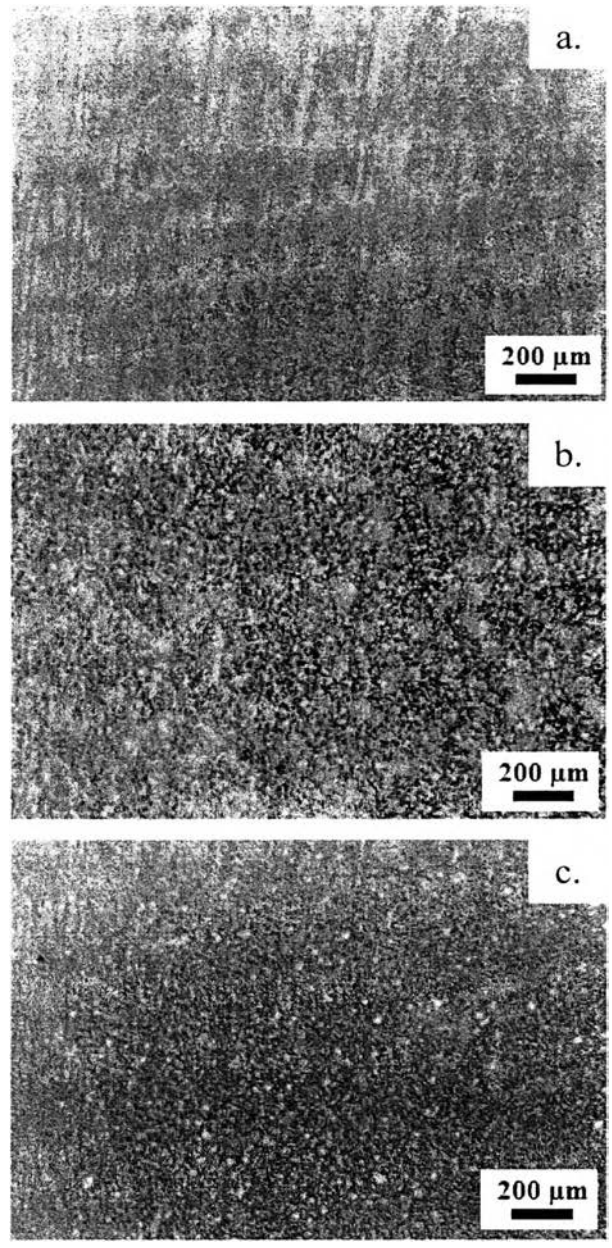

Figure 5.2 Optical microscopy images of (a) P25 TiO_2electrode, (b) P25 TiO_2/purified Na-bentonite electrode, and (c) P25 TiO_2/CTAB-modified Na-bentonite electrode.